Mechanical relaxations and moduli of oriented semicrystalline polymers

W. P. Leung, C. C. Chan, F. C. Chen and C. L. Choy
Department of Physics The Chinese University of Hong Kong, Hong Kong
(*Received* 20 *November* 1979; *revised* 17 *June* 1980)

A systematic investigation was carried out on the mechanical relaxations and moduli of four drawn semicrystalline polymers: polyoxymethylene, polypropylene, polyvinylidene fluoride and polychlorotrifluoroethylene. Low-frequency tensile and torsional measuremnts were made between -140 and 140°C, and ultrasonic measurements of all five moduli were made by the water-tank method between 0 and 60°C. The patterns of relaxations remain essentially unchanged upon orientation, but there is a marked reduction of the height of relaxation peaks associated with the amorphous phase and, correspondingly, a smaller drop of moduli in the relaxation region. This reflects a lowering of molecular mobility in the amorphous phase due to the constraining effect of taut tie-molecules. The modulus C_{33} increases sharply with draw ratio λ while the other moduli show little variation, which result from the alignment of molecular chain axes and the production of taut tie-molecules. The λ-dependence of the moduli is consistent with the aggregate model only when the polymer is glassy, that is, when its amorphous phase is comparable in stiffness to the crystalline phase and the polymer can reasonably be regarded as a one-phase material for which the aggregate model is valid.

INTRODUCTION

Recently considerable work[1-17] has been done on the elastic moduli and mechanical relaxations of oriented polymers. The investigations have been concentrated on the highly crystalline polymers: high-density polyethylene (HPDE), polyoxymethylene (POM) and polypropylene (PP), which can be oriented by drawing or extrusion to draw ratio as high as 20–30. These processes produce materials of ultra-high axial modulus, which are of great practical interest. Most static and low-frequency measurements have been made on the axial Young's modulus E_0[2-13], and recently Ward and co-workers[14-17] have also studied mechanical relaxations by both dynamic tensile and torsional measurements. In the high-frequency region (2–35 MHz) ultrasonic measurments have been made on PP[18,19] and HDPE[20]; there has also been work on oriented polymers of relatively low crystallinity, i.e. polyvinyl chloride (PVC)[21] and polyethylene terephthalate (PET)[18].

The gross features of the draw ratio (λ) dependence of the elastic moduli revealed by these studies are quite simple: a sharp and continued rise of the tensile modulus along the draw direction $\hat{z}$ and relatively little change in the other moduli as λ increases. However, attempts to understand these features in greater detail by the use of a model (such as the aggregate model) had mixed success.

Systematic investigations of the dynamic mechanical properties of a number of polymers over a wide frequency and temperature range are needed, so that a pattern of general behaviour may emerge. In this work we study four polymers of widely different crystallinity χ: POM ($\chi = 0.63$), PP ($\chi = 0.62$), polyvinylidene fluoride (PVF_2, $\chi = 0.48$) and polychlorotrifluoroethylene (PCTFE, $\chi = 0.40$). The work included low-frequency measurements on the torsional modulus G about the draw axis $\hat{z}$ of the oriented sample by use of a torsional pendulum at 1 Hz, and on the axial Young's modulus E_0 by use of a viscoelastic spectrometer at 10 Hz, with the corresponding loss factors tan δ for the two moduli, over the temperature range −140 to 140°C. It also included 10 MHz ultrasonic measurements on all five elastic moduli C_{AB} of the transversley isotropic sample and one of the loss factors by the water-tank method between 0 and 60°C.

The results have been interpreted in the light of structural changes which take place during orientation, with emphasis on the effects of temperature, frequency and draw ratio. It was found that the time–temperature equivalence rule which relates high- and low-frequency data is approximately correct, even though a shift of 55–120°C in temperature is involved in making the comparison. The λ-dependence of the complete set of five elastic moduli obtained from ultrasonic measuremnts was analysed in the framework of the aggregate model. The model is found to be applicable when the semicrystalline polymer can reasonably be regarded as a one-phase material, that is, when its amorphous phase is glassy and comparable to the crystalline phase in stiffness.

There have been a number of published methods[21-23] for analysing the results of ultrasonic measurements on anisotropic samples with cylindrical symmetry. The analysis carried out in this work follows a slightly different path. Discussion of the results is separated into two parts, the first part dealing with low-frequency data and mechanical relaxations, and the second part with ultrasonic data and the aggregate model.

0032-3861/80/101148-13$02.00

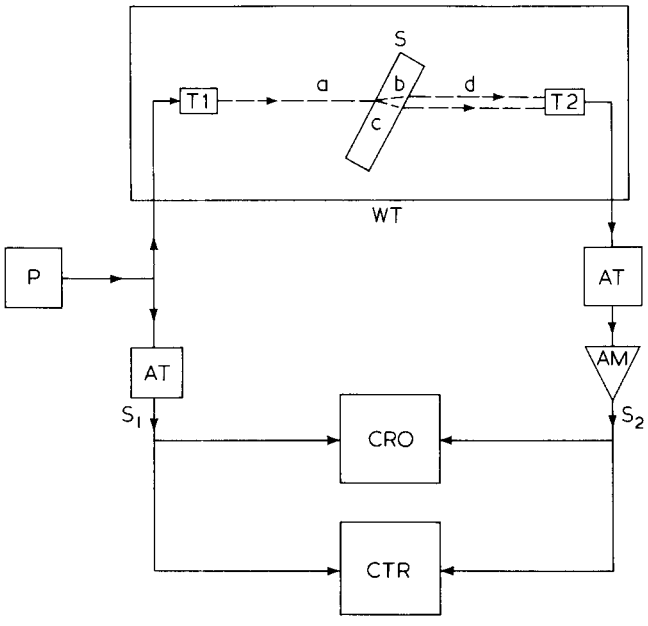

Figure 1 Schematic diagram of the experimental setup for ultrasonic measurements by the water-tank method. P, pulser; T1, transmitting transducer; T2, receiving transducer; S, sample; a, incident ultrasonic beam; b, refracted beam of longitudinal wave; c, refracted beam of transverse wave; d, transmitted beams. Sample and transducers immersed in water within the tank (WT). AT, attenuator; AM, wide-band amplifier; CRO, oscilloscope; CTR, time-interval counter; S1, triggering signal for CRO and start signal for the counter; S2, signal viewed on CRO and stop signal for the counter

EXPERIMENTAL

Sample preparation

The starting material for PP (Hostalen PPK) and PCTFE (Kel-F) samples were supplied in the form of pellets by Hoechst Co. and the 3M Co., respectively; that for the PVF_2 samples was supplied by Cellomar Associates, Inc. in the form of powder. Isotropic sheets for these polymers were prepared by compression moulding at $\sim 30°C$ above the the melting point and then quenched in water at room temperature. The 3 mm sheets of POM (Delrin) supplied by DuPont were used as received.

To prepare oriented samples, dumb-bell shaped sample sheets of gauge length 3 cm and width 1.5–2.5 cm were drawn on an Instron tensile machine, fixed draw temperature of 150, 130 and 90°C being used for all samples of POM, PP and PVF_2, respectively. The 'natural draw ratio' of PCTFE increases with draw temperature, and so this polymer was drawn at 2 cm min^{-1} at temperatures of 22, 60 and 90°C for $\lambda = 1.8$, 3 and 4, respectively. The draw rate used for the other three polymers depends on the draw ratio λ: for λ not exceeding the natural draw ratio (which is ~ 5, 5.5 and 4 for POM, PP and PVF_2, respectively) a 'low rate' of 1 mm min^{-1} was used to ensure that the sample is homogeneously drawn along the entire length; for higher λ (in case of POM and PP) the sample was first drawn to the natural draw ratio at a 'fast rate' of 2cm min^{-1}, then cut to ~ 2 cm gauge length for a second-stage drawing at the rate of 1 mm min^{-1} (i.e. $< 10\%$ min^{-1}) until the desired λ is achieved as suggested by Clark and Scott[6]. The drawn samples were stored for at least two days before measurements were taken, and those for ultrasonic measurements were annealed at 80°C for 2 h to prevent shrinking during experiment. Preliminary measurements have shown that such an annealing procedure has little effect ($< 3\%$) on all the observed moduli.

The flotation method was used to determine the density, which together with the literature values of the densities of the amorphous and the crystalline phase[24-27] allowed a determination of the volume fraction crystallinity χ, yielding 0.63, 0.62, 048 and 0.40 for isotropic samples of POM, PP, PVF_2 and PCTFE, respectively. χ does not change appreciably for drawn samples, except for the PP sample of $\lambda = 22$, which has a relatively low density and a white and silky appearance, probably indicating the presence of microvoids.

The thickness of the oriented sheets varied from 0.4 to 2 mm, depending on draw ratio. They were cut into 1.2×1.5 cm rectangles for ultrasonic measurements, and into strips 5 cm long and 0.5–0.6 mm wide (the aspect ratio being such as to ensure the absence of the end effect[28]) for tensile and torsional measurements.

Ultrasonic measurement

The setup for ultrasonic measurement by the water-tank method is very similar to that described by Rawson and Rider[21]. The sample and the transmitting and receiving transducers (Panametrics) were suspended from a platform with angle-adjustment mechanisms, which in turn was supported by a frame standing at the bottom of a tank filled with water (*Figure* 1). The water temperature varying between 0 and 60°C was controlled to within 0.1°C by a heater unit (Techne) and was sensed by a thermocouple attached to the sample holder.

A pulse generator (Panametrics 5052PR) energized the submerged piezoelectric ceramic transmitting transducer which generated a beam of pulsed 10 MHz ultrasonic waves in water, each pulse lasting 1 μs and the repetition rate being 5 kHz. The beam impinged on an oriented sample at a set angle and generated both a longitudinal and a transverse wave within the sample which were subsequently refracted back into water and picked up by a receiving transducer. The received signals and attenuated driving pulse were observed on a Tektronix 7834 Oscilloscope, and the transit time t for the ultrasonic pulse to travel from one transducer to the other was measured on a gated interval-counter with a resolution of 0.2 ns (Tektronix 7D15). The determination of ultrasonic velocities in the sample and the computation of its elastic moduli will be described in the next section.

The attenuation coefficient α of the sample was determined by comparison of the amplitude of a pulse transmitted through the sample at normal incidence with that of the received pulse when the sample was removed. Reflection at the sample surfaces requires corrections of $\sim 10\%$, but interference effects can be neglected, since the pulse width is shorter than the transit time through the sample.

Low-frequency measurements

Dynamic tensile measurement of the oriented samples along the draw-direction was carried out on a viscoelastic spectrometer (Iwamoto Seisakusho Ltd.), which determined both the Young's modulus E_0 and the loss factor $\tan\delta$ at a frequency of 10 Hz and at temperatures between -140 and 140°C.

Dynamic torsional measurement about the draw-axis of the oriented samples was carried out on a torsional pendulum of the inverted type similar to that of Gray and McCrum[29]. The cylindrical sample chamber together

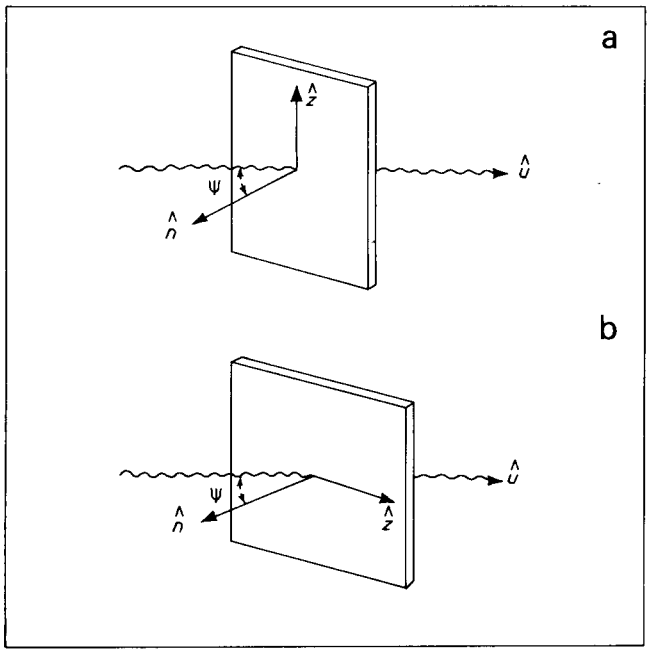

Figure 2 Schematic diagram showing the relative orientations of the direction of the incident ultrasonic beam $\hat{u}$, the normal $\hat{n}$ to the sample surface and the draw direction $\hat{z}$ in two arrangements: (a) for the measurement of C_{11} and C_{66}, and (b) for that of C_{13}, C_{33} and C_{44}

with its heater was surrounded by a brass enclosure immersed in liquid nitrogen, allowing for a variation of temperature between −140 and 140°C. Adjustment of the moment of inertia by adding weights to the moment arm kept the frequency of torsional motion constant to within 5% of 1 Hz. The motion was recorded on a Photodyne Recorder, which followed the movement of a light beam reflected from a mirror attached to the axis of the moment arm.

ANALYSIS OF DATA

The determination of the dynamic Young's modulus E_0, the shear modulus $G\,(=C_{44})$ and the corresponding loss factors tan δ from low-frequency experiments follow a standard procedure[30] and need not be elaborated here.

The analysis of the water-tank data is more complicated since four series of ultrasonic velocities are involved. The determinations of C_{11} and C_{66} are directly related to the velocities of the longitudinal wave (v_1) and transverse wave (v_2) respectively, generated in the oriented sample when it is aligned so that the draw direction $\hat{z}$ is normal to the plane of the ultrasonic beam direction $\hat{u}$ and the normal to the sample surface $\hat{n}$ (*Figure 2a*):

$$C_{11}=\rho v_1^2 \qquad (1)$$

$$C_{66}=\rho v_2^2$$

where ρ is the sample density. In this case v_r $(r=1,2)$ should be independent of the incident angle ψ if the uniaxially drawn sample is transversely isotropic. By comparing results of several measurements at different ψ (leading to different acoustic path within the sample) this was found to be the case, and these results are averaged for an accurate determination of C_{11} and C_{66}, and hence the linearly dependent C_{12} $(=C_{11}-2C_{66})$.

When the sample is so aligned that the draw direction $\hat{z}$ lies in the same plane as $\hat{u}$ and $\hat{n}$ (*Figure 2b*) then the velocities of the two waves (v_3 for the quasi-longitudinal wave and v_4 for the quasi-transverse wave) generated in the sample are dependent on the incident angle, and are related to four of the five independent elastic moduli. For a given incident angle ψ these two velocities satisfy the Musgrave equation[31], which can be written in the following form:

$$y^2+a_1xy+a_2x^2+a_3y+a_4x=0 \qquad (3)$$

where

$$y=\rho v_r^2-C_{11} \qquad (r=3,4) \qquad (4)$$

$$x=\sin^2\theta_r \qquad (5)$$

θ_r being the angle of refraction for the wave concerned and related to the angle of incidence ψ through Snell's law:

$$\frac{\sin\psi}{v_w}=\frac{\sin\theta_r}{v_r} \qquad (r=3,4) \qquad (6)$$

The coefficients a_n are combinations of the moduli: $a_1=C_{11}-C_{33}$, $a_2=(C_{13}+C_{44})^2-(C_{11}-C_{44})(C_{33}-C_{44})$ and $a_3=C_{11}-C_{44}$; $a_4=a_1a_3-a_2$ is not independent. Thus once C_{11} has been measured one can compute the variables (x,y) from the measured velocities v_r $(r=3,4)$ at different angles of incidence according to equations (4) and (5). Then a_n $(n=1,2,3)$ and hence the moduli C_{13}, C_{33} and C_{44} can be determined by a least-squares fit of equation (3) to these points (see the Appendix for details). The overall accuracy of C_{AB} is estimated to be 3–7%, which reflects the uncertainty in angle and time measurements, as well as in the thickness of the samples.

From the five elastic moduli C_{AB} one can readily compute the compliance constants S_{AB} by usual matrix inversion, and also obtain the moduli commonly measured, i.e. the Young's moduli E_0 (along $\hat{z}$) and E_{90} (normal to $\hat{z}$) and the torsional modulus G about $\hat{z}$, which are $1/S_{33}$, $1/S_{11}$ and C_{44}, respectively. The comparison of high- and low-frequency results for the same polymer can therefore be easily made.

From the attenuation coefficient of α of the sample determined in the last section, the loss factor tan δ can be calculated through the relation

$$\tan\delta=\frac{\alpha\lambda}{\pi}$$

where λ is the wavelength of the ultrasonic wave in the sample.

RESULTS AND DISCUSSIONS

Mechanical relaxations

Results of the dynamic torsional measurements about the draw-axis are shown in *Figures* 3–6 for POM, PP, PVF_2 and PCTFE, respectively. The isotropic samples exhibit two to four relaxations. The α peak is known[30] to originate from the crystalline regions, and is also the most prominent. However, it is absent in PCTFE, which is understandable since the crystallinity of the sample is only

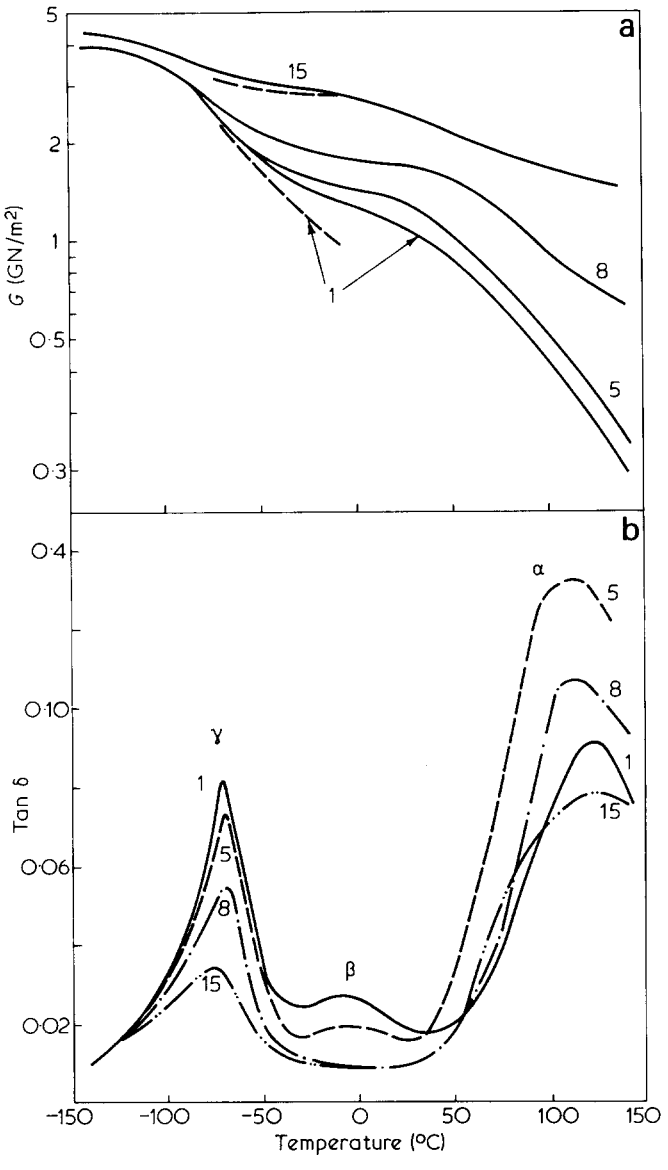

Figure 3 Temperature dependence of (a) the shear modulus G (—) and (b) the loss factor tan δ of POM for λ = 1, 5, 8 and 15, as obtained from torsional measurements at 1 Hz. G obtained from ultrasonic measurements at 10 MHz for λ = 1 and 15 at 0–60°C have been shifted by −70°C and shown as dashed lines (– – –) in (a)

0.4. The β-relaxation for PP and PCTFE is associated with the glass–rubber transition in the amorphous region. In the cases of POM and PVF_2 both the β and the γ relaxation arise from chain motions in the amorphous region, but there is still some controversy as to which is related to the glass transition. Recently Boyer[32] assigned the β and γ transitions of PVF_2 as the upper and lower glass transitions, respectively. The assignment for POM is still uncertain[30,32] and we tentatively associate the γ-peak with the glass-transition since it is prominent and there is a jump in thermal expansivity at about the same temperature.

The same features of relaxation are observed in the oriented samples, which imply that similar molecular processes are involved. We note that all relaxation peaks associated with the amorphous region decrease in magnitude upon orientation and, in the cases of PVF_2 and PCTFE, also shift upwards in temperature. In fact, the β peaks of various heights observed in the isotropic samples of POM, PP and PVF_2 all disappear at sufficiently high draw-ratio. This apparently results from reduction of molecular mobility in the amorphous region owing to the presence of strained tie-molecules. The crystallites in isotropic PVF_2 are mainly of the α (helical) from[33], which change into the β (planar zigzag) form upon orientation, however this does not seem to affect the location of the peaks.

Orientation has relatively little effect upon the torsional modulus G at low temperature (say −100°C), whereas the effect becomes considerable for the highly drawn samples above the major amorphous relaxations. This is because, for the isotropic sample, G drops drastically at the relaxation region, but the drop is much smaller when the draw ratio λ exceeds 5. These features can be attributed to the stiffening effect of the taut tie-molecules, the importance of which increases continuously with λ.

Results of the dynamic tensile measurements along the draw-axis as shown in *Figures* 7–10 have features similar to

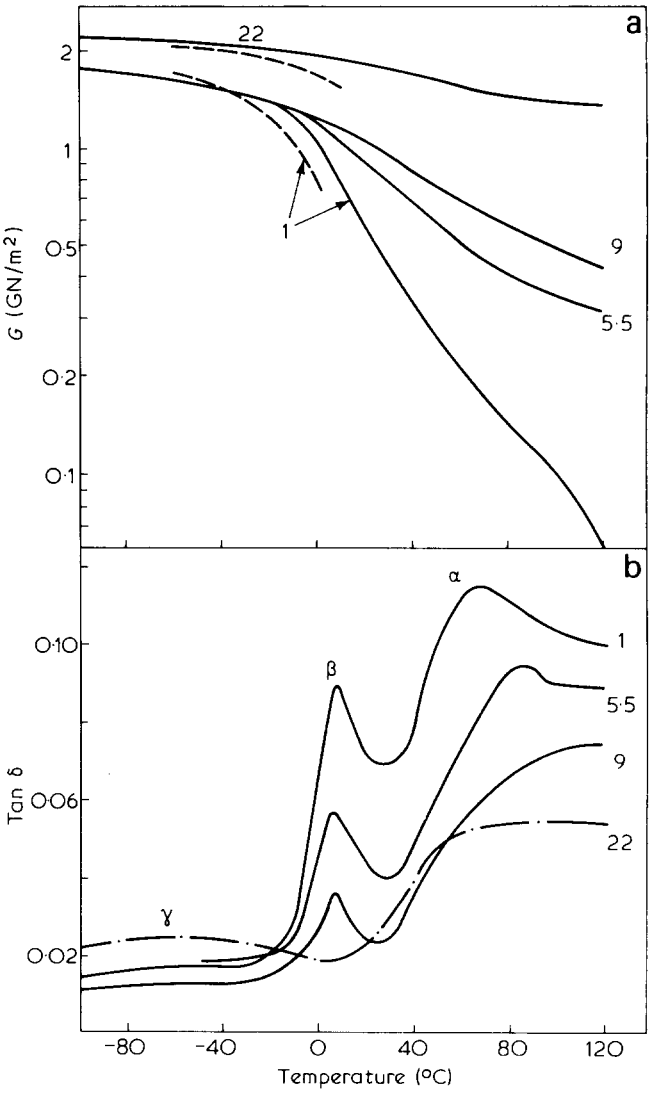

Figure 4 Temperature dependence of (a) the shear modulus G (—) and (b) the loss factor tan δ of PP for λ = 1, 5.5, 9 and 22, as obtained from torsional measurements at 1 Hz. G obtained from ultrasonic measurements at 10 MHz for λ = 1 and 22 at 0–60°C have been shifted by −55°C and shown as dashed lines (– – –) in (a)

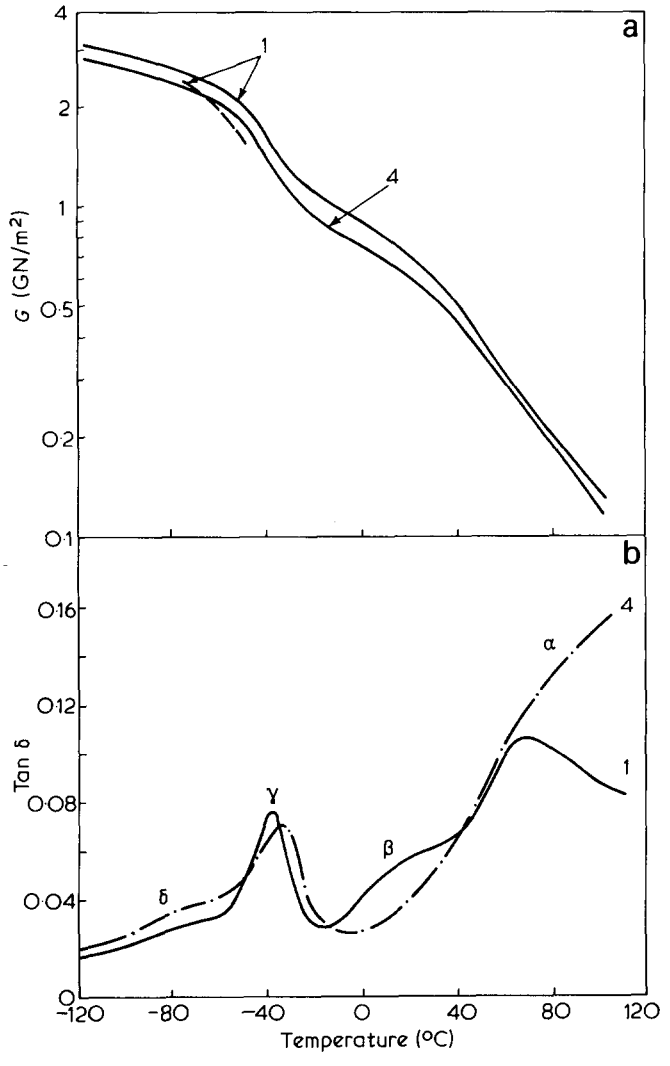

Figure 5 Temperature dependence of (a) the shear modulus G (—) and (b) the loss factor tan δ of PVF_2 for $\lambda = 1$ and 4, as obtained from torsional measurements at 1 Hz. G obtained from ultrasonic measurements at 10 MHz for $\lambda = 1$ at 0–30°C has been shifted by −75°C and shown as dashed lines (— — —) in (a)

those for the torsional measurements. It is seen that the axial Young's modulus E_0 increases rapidly with λ, which is understandable since the increasing alignment of strong covalent bonds along the draw-axis should have a direct enhancement effect on E_0. The drop in E_0 at the major amorphous relaxation is relatively small for the highly drawn samples, with the result that the λ-dependence is even stronger at high temperature. Generally our dynamic mechanical measurements on oriented samples of POM and PP obtained by two-stage drawing are consistent with previous studies of Ward and co-workers[14,15] on single-stage drawn materials, indicating that the two sets of samples probably have similar structures.

The shear modulus G obtained from ultrasonic measurements is superimposed on the corresponding low-frequency results in *Figures* 3–6, and similarly the ultrasonic Young's modulus E_0 is also shown in *Figures* 7–10. To account for the differences in frequency, we use the well-known time-temperature equivalence and the relaxation peak positions observed at different frequencies (including data from refs 34–36) to shift the ultrasonic data to lower temperatures. There is a 5–30% agreement between the ultrasonic and the low-frequency data, which is quite good in view of the approximate nature of the rule for time–temperature equivalence and the large difference in frequencies involved.

Measurements on the velocity and attenuation of ultrasonic longitudinal wave propagating normal to the draw-axis were made, and the resulting modulus C_{11} and loss factor tan δ are shown in *Figures* 11–13. As expected, the glass–rubber transitions of POM, PP and PVF_2 have been shifted up to 0, 65 and 40°C, respectively. All the relaxations of PCTFE have shifted to above our temperature range therefore the data are not presented. The loss factor tan δ decreases for increasing λ, again demonstrating the stiffening effect of tie-molecules in the amorphous region. In contrast to the case for E_0, the orientation process causes a decrease in C_{11} at low temperature, simply because the process aligns the strong covalent bonds normal to the direction of wave propagation. However, the isotropic samples have a bigger drop of C_{11} at the amorphous relaxations than the oriented samples (also suggested by the difference in the peak height of tan δ), thus causing a cross-over of the modulus in this region and a reversal of their relative magnitudes at high temperature.

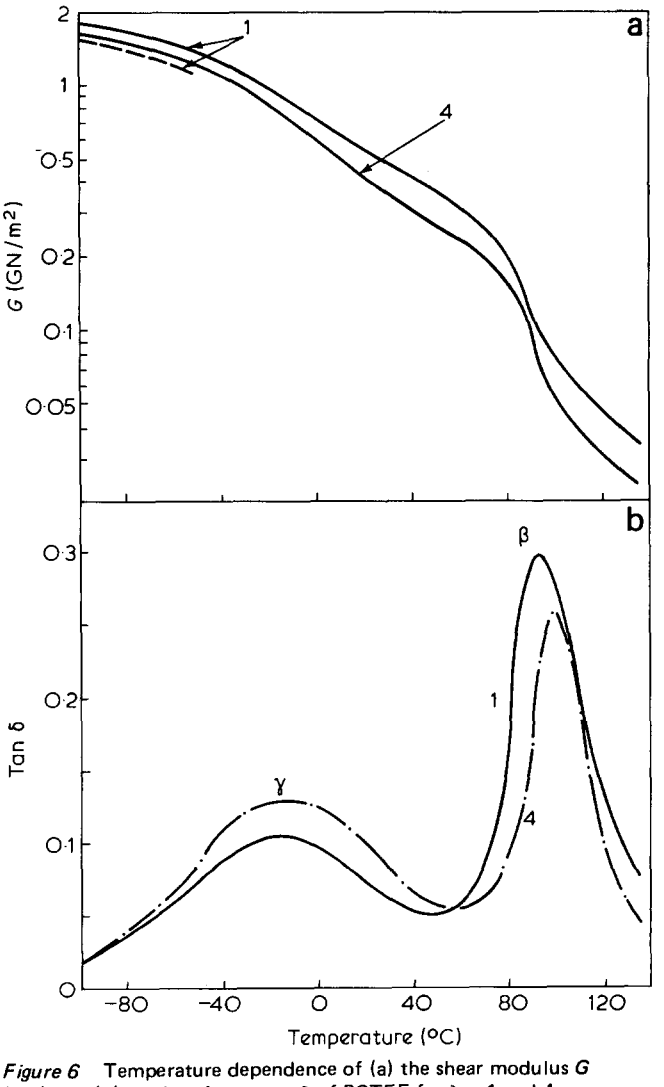

Figure 6 Temperature dependence of (a) the shear modulus G (—) and (b) the loss factor tan δ of PCTFE for $\lambda = 1$ and 4, as obtained from torsional measurements at 1 Hz. G obtained from ultrasonic measurements at 10 MHz for $\lambda = 1$ at 0–50°C has been shifted by −120°C and shown as dashed lines (— — —) in (a)

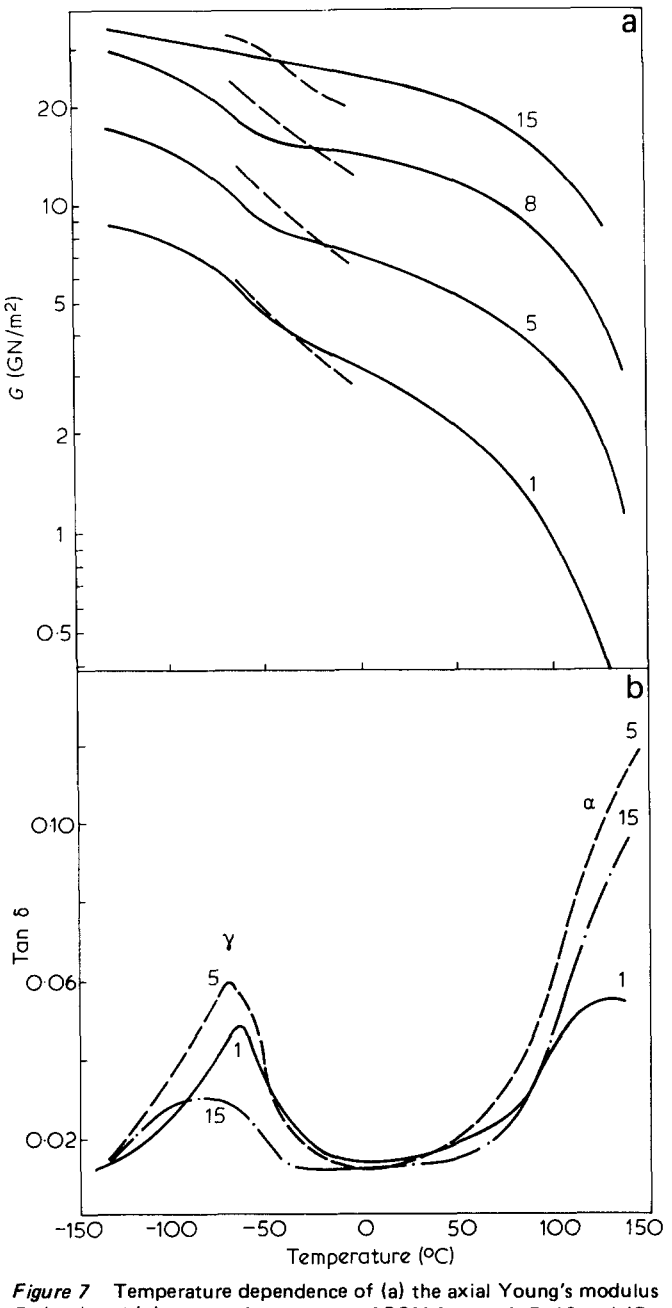

Figure 7 Temperature dependence of (a) the axial Young's modulus E_0 (—) and (b) the loss factor tan δ of POM for λ = 1, 5, 10 and 15, as obtained from dynamic tensile measurements at 10 Hz. tan δ for λ = 10 is not shown. E_0 obtained from ultrasonic measurements at 10 MHz at 0–60° C have been shifted by −65° C and shown as dashed lines (— — —) in (a)

Elastic moduli

Results of the ultrasonic measurements on the elastic moduli C_{AB} are shown as functions of draw ratio at fixed temperatures in *Figures* 14–19, and the moduli E_0, E_{90} and G ($=C_{44}$) are given in *Table* 1. For the two highly oriented polymers, POM and PP, both 0 and 60°C data are presented. Only 0°C data are presented for PVF_2 and PCTFE, since the moduli of PCTFE have only weak temperature dependence in this range and shear wave measurement of PVF_2 cannot be made above 20°C because of strong attenuation. There is a large, steady rise of the value of C_{33} for all samples, which increases two fold from $\lambda = 1$–5 and four fold from $\lambda = 1$–20. Above the major amorphous relaxations the shear modulus C_{44} shows fairly large increase for $\lambda \leqslant 10$. The other three moduli C_{11}, C_{12} and C_{13} have relatively small λ-dependence, changing by no more than 10–20% throughout the range. The moduli for the $\lambda = 22$ PP sample have anomalously low values, probably due to the presence of microvoids in this sample as previously mentioned.

Qualitatively these general features are what one might expect from the structural changes in drawn semicrystalline polymers, which have been studied by X-ray, birefringence and other experimental techniques[17,37–39]. Firstly there is a partial alignment of the molecular chain-axes along the draw-direction $\hat{z}$, leading to a rise of the stiffness along this direction and a drop in the perpendicular direction. At the same time the spherulites are being broken up into smaller crystalline blocks, which are connected by inter-crystalline bridges, forming stacks aligned along $\hat{z}$. In the case of high-density polyethylene it has been found that the volume fraction of these bridges continues to increase up to the highest attainable draw-

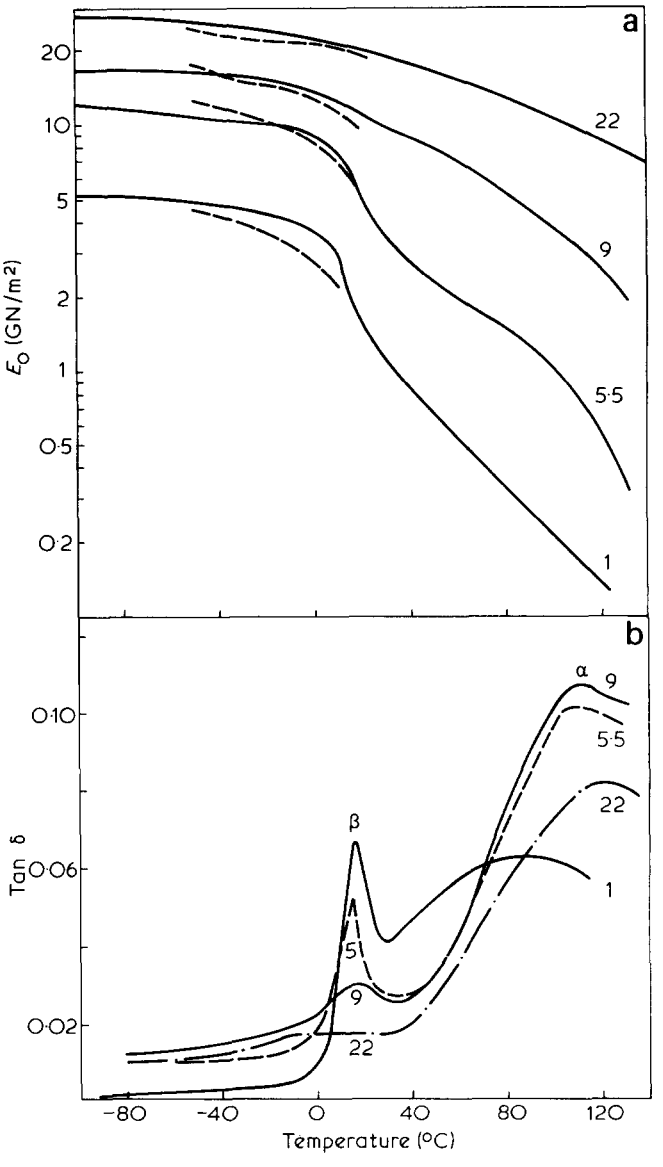

Figure 8 Temperature dependence of (a) the axial Young's modulus E_0 (—) and (b) the loss factor tan δ of PP for λ = 1, 5.5, 9 and 22, as obtained from dynamic tensile measurements at 10 Hz. E_0 obtained from ultrasonic measurements at 10 MHz at 0 to 60° C have been shifted by −50° C and shown as dashed lines (— — —) in (a)

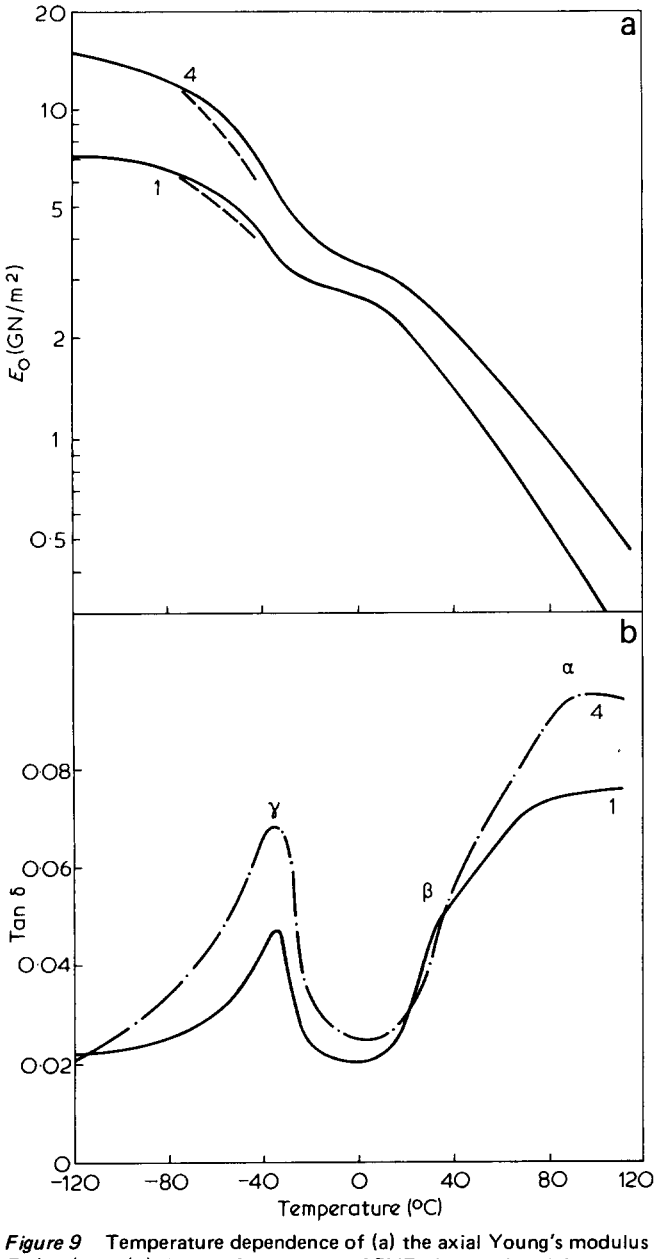

Figure 9 Temperature dependence of (a) the axial Young's modulus E_0 (—) and (b) the loss factor tan δ of PVF_2 for λ = 1 and 4, as obtained from dynamic tensile measurements at 10 Hz. E_0 obtained from ultrasonic measurements at 10 MHz at 0–30°C have been shifted by −70°C and shown as dashed lines (— — —) in (a)

ratio[17], and so their reinforcing effect would account for the continued increase of C_{33} above $\lambda = 5$, at which point the alignment of the chain-axes in the crystallites is almost complete.

At present there is no realistic framework in which the effect of the above complex morphological changes on all the elastic moduli can be calculated. A popular model which allows some quantitative analysis of the situation is the modified Takayanagi model[17,40,41] which, however, cannot be applied readily to the polymers studied in this work due to lack of data on the volume fraction of the crystalline bridges. In order to make some phenomenological correlation of the results obtained we can only resort to the other commonly used model — the aggregate model[42,43], which attempts to account for the changes in moduli in terms of the alignment of microscopic units with fixed intrinsic moduli. Such an analysis seems meaningful in the temperature region below the glass transition, where the stiffness of the amorphous and crystalline phases are not so different and the polymer may reasonably be regarded as a one phase material.

The model assumes that a polymer is composed of identical transversely isotropic microscopic units, each with intrinsic elastic moduli C^u_{AB}, and that the process of drawing only produces a preferential distribution in the orientation of these units. For a given distribution one may take the ensemble average of the moduli C^u_{AB} to obtain the 'Voigt average' C^v_{AB} for the macroscopic moduli, from which the corresponding compliance S^v_{AB} can be calculated. Also one may take the ensemble average of the unit compliance S^u_{AB} to obtain the 'Reuss average' S^R_{AB} for the macroscopic compliance, and hence obtain the corresponding moduli C^R_{AB} as well. Since there

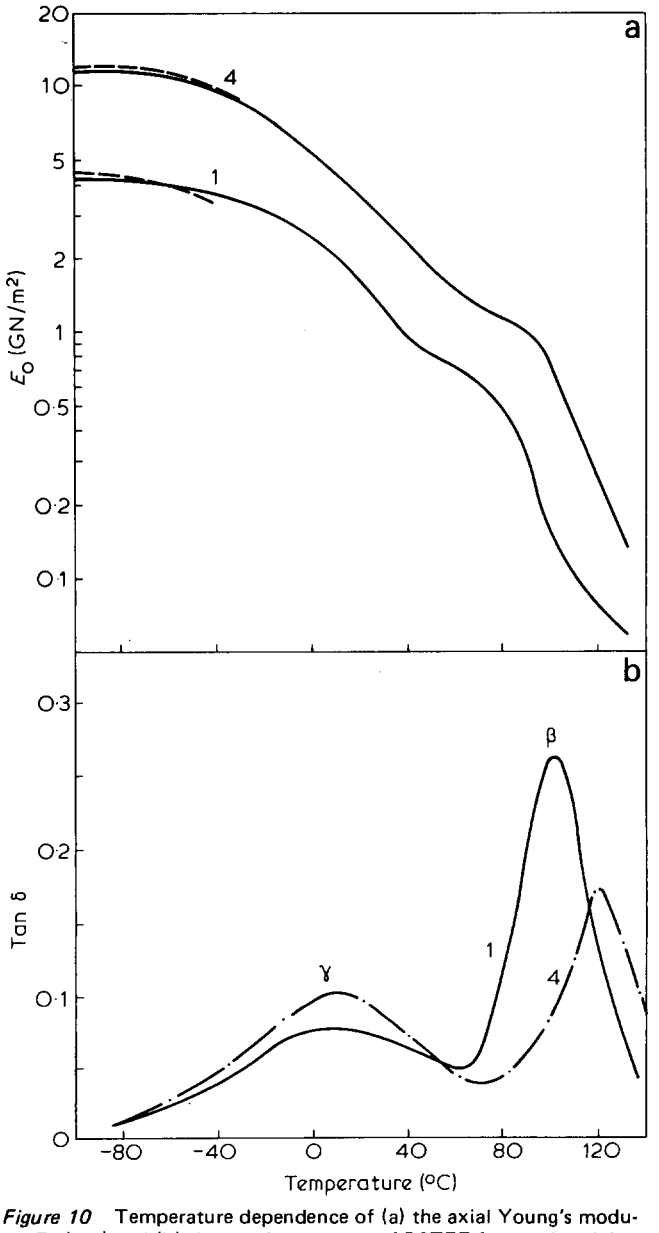

Figure 10 Temperature dependence of (a) the axial Young's modulus E_0 (—) and (b) the loss factor tan δ of PCTFE for λ = 1 and 4, as obtained from dynamic tensile measurements at 10 Hz. E_0 obtained from ultrasonic measurements at 10 MHz at 0–50°C have been shifted by −100°C and shown as dashed lines (— — —) in (a)

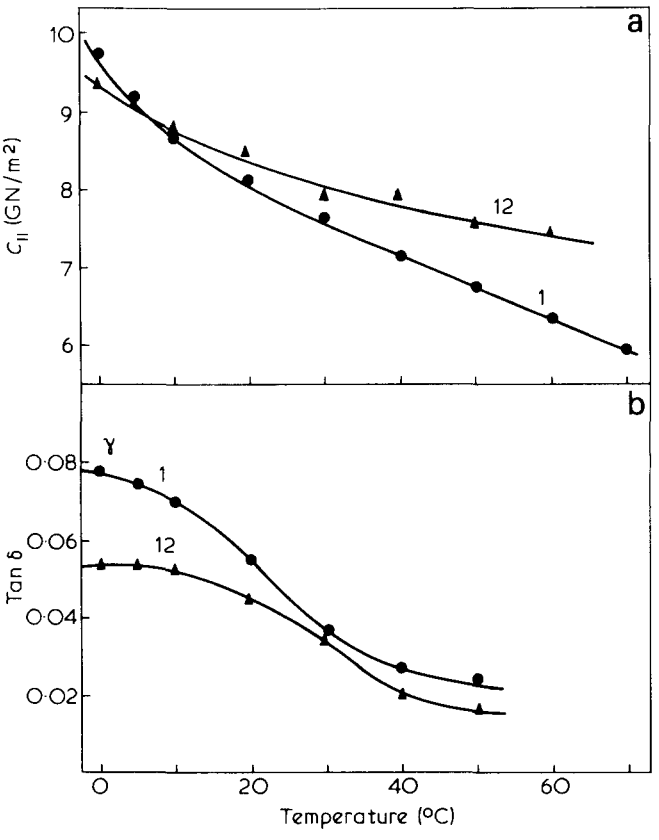

Figure 11 Temperature dependence of (a) C_{11} and (b) the corresponding loss factor tan δ of POM for λ = 1 and 12 as obtained from ultrasonic measurement at 10 MHz.

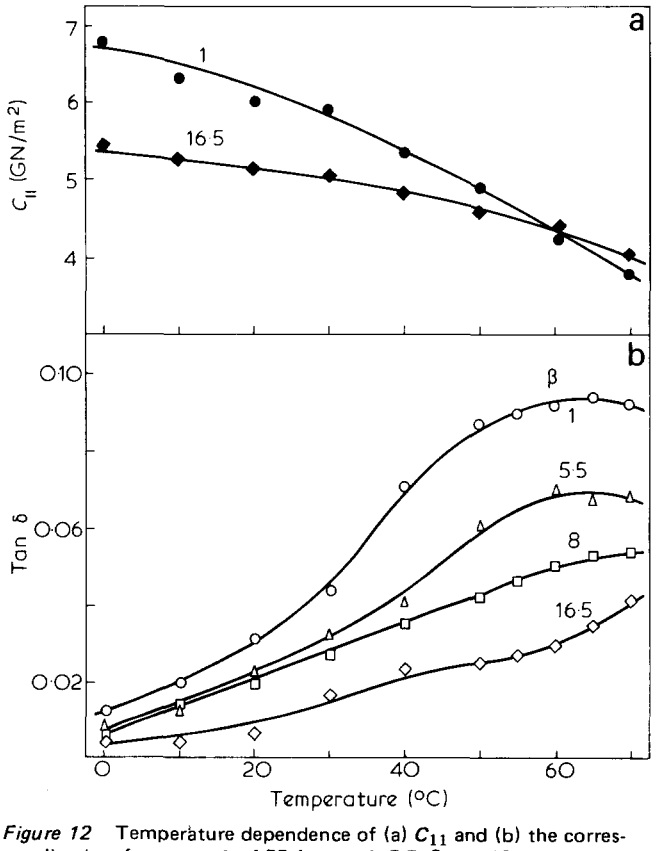

Figure 12 Temperature dependence of (a) C_{11} and (b) the corresponding loss factor tan δ of PP for λ = 1, 5.5, 8 and 16.5, as obtained from ultrasonic measurement at 10 MHz. C_{11} for λ = 5.5 and 8 are not shown

is no prescription for the mechanical coupling of the differently oriented microscopic units, the macroscopic moduli C_{AB} are expected to lie between the Voigt (upper) and Reuss (lower) bounds.

To apply the model to our data the intrinsic moduli C^u_{AB} must firstly be deduced. It is expected that at very high draw ratio such units would be mostly aligned along $\hat{z}$ and the observed moduli would be close to C^u_{AB}. It has been found that a convenient way of obtaining C^u_{AB} was by least-squares fitting a polynomial of the empirical form $a + b/\lambda^2$ to the high draw-ratio data and extrapolating the resulting polynomial to $\lambda = \infty$. Secondly, a specific assumption about the distribution of the orientation of the units must be made. The pseudo-affine deformation is a commonly used scheme, which assumes that the symmetry axes of the microscopic units rotate in the same manner as lines joining material points in the sample, which deforms at constant volume. On the basis of these two assumptions we obtain Voigt and Reuss bounds for all five moduli C_{AB} of POM and PP at 0 and 60°C, which are plotted in *Figures* 14–17 along with the data. It is apparent that there is agreement between the data and the bounds in the general trends of λ-dependence, e.g. the sharp rise in C_{33}, the moderate fall in C_{11} and the approximate constancy (excepting C_{44}) of other moduli. However, the data for

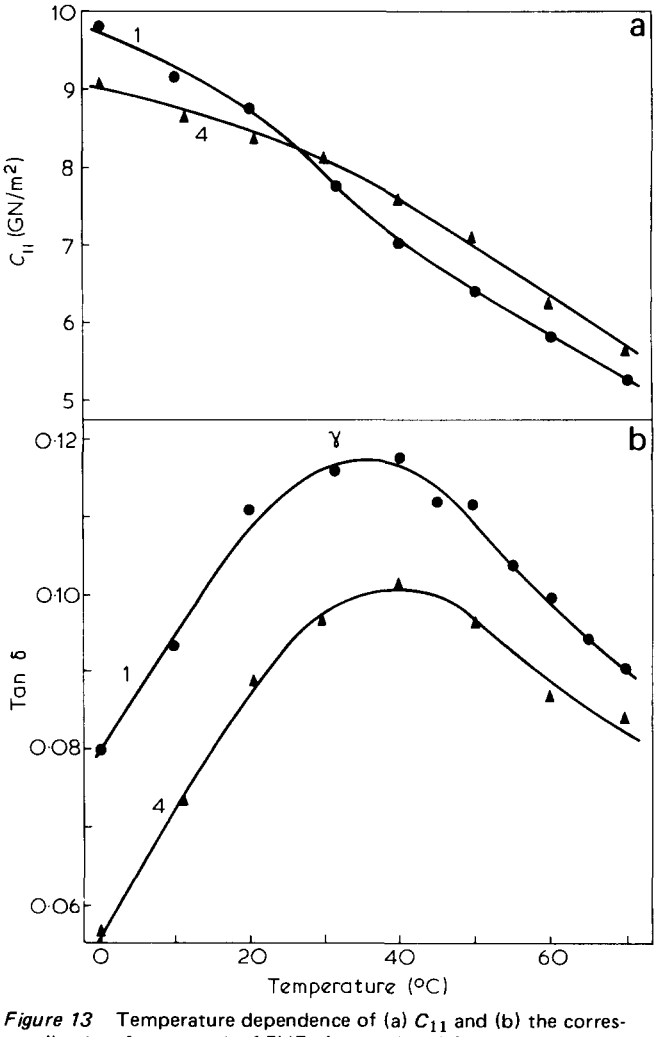

Figure 13 Temperature dependence of (a) C_{11} and (b) the corresponding loss factor tan δ of PVF_2 for λ = 1 and 4, as obtained from ultrasonic measurement at 10 MHz.

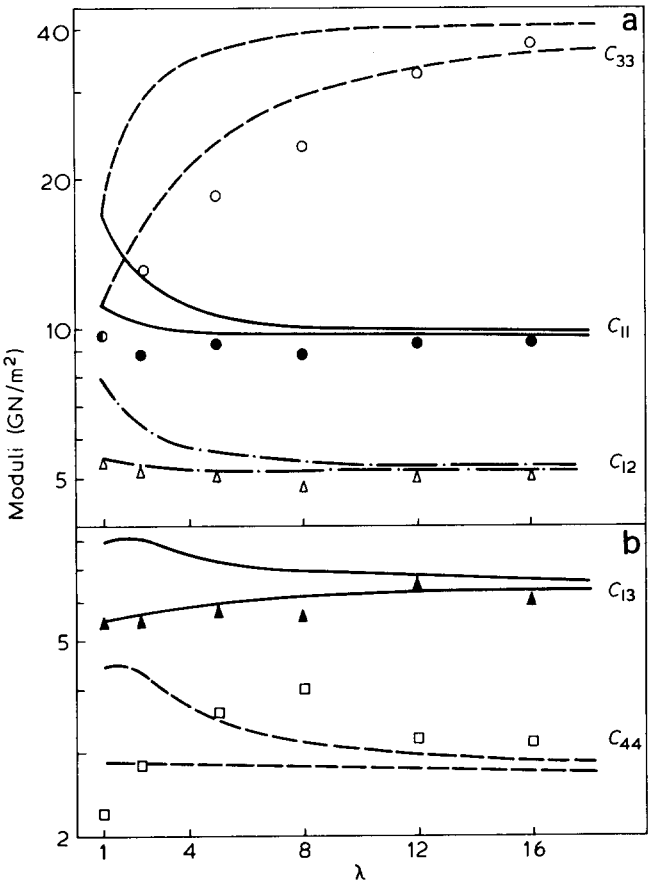

Figure 14 Draw ratio dependence of (a) C_{11} (●), C_{12} (△), C_{33} (○) and (b) C_{13} (▲), C_{44} (□) of POM at 0°C, obtained by ultrasonic measurement at 10 MHz. The Voigt (upper) and Reuss (lower) bounds calculated according to the aggregate model for each of the moduli are shown along with the data points: – – – – for C_{33} and C_{44}, —— for C_{11} and C_{13}, – · – · – for C_{12}

POM and those for PP at 60°C are mostly below the lower bounds whereas those for PP at 0°C essentially lie on the lower bounds, in agreement with our previous work on extruded PP[18]. The explanation probably lies in the difference of the glass-transition temperature at the frequency of our measurements (10 MHz), which is ~0 and 65°C for POM and PP, respectively. Thus the amorphous phase is rubbery or nearly rubbery except for the PP samples at 0°C. It is reasonable that a one-phase model such as the aggregate model can only be applied to PP at 0°C, for which the two phases have similar stiffness.

We can also apply the model in a more general manner, without explicit use of the intrinsic moduli C^u_{AB} or a specific deformation scheme. Bounds on the moduli of the isotropic sample can be obtained from the moduli of an oriented sample at any draw ratio by treating the latter as the intrinsic moduli of the microscopic unit in a random aggregate[42]. This allows an analysis of data on polymers such as PVF_2 and PCTFE for which C^u_{AB} cannot be deduced because they cannot be highly oriented. The results are plotted in *Figures* 20–22, where it is seen that the measured moduli of the isotropic samples of PVF_2 and PP at 0°C are within the predicted bounds, whereas those of POM (0 and 60°C) and PP (60°C) are outside the bounds. The 0°C data for PCTFE are below the lower bounds by 5–10%, which is comparable with experimental error. Recalling that the glass-transition temperatures for both PVF_2 and PCTFE are well above 0°C at 10MHz, one may again invoke the relaxational behaviour of these polymers to account for the above results, which seem to obey a general rule[18,44] that the aggregate model can be applied to an oriented semicrystalline polymer when its amorphous phase is glassy, but not when it is rubbery or nearly rubbery.

This rule also applies to two of the five polymers previously studied at room temperature by static measurements[44,45]: as expected, data for polyethylene terephthalate (glass-transition temperature $T_g \simeq 70°C$) are inside bounds predicted by the aggregate model whereas those for PP ($T_g \simeq -10°C$) are outside the bounds. Data for high-density polyethylene (T_g below room-temperature) and Nylon 66 ($T_g \simeq 70°C$) also seem to be consistent with the rule if the experimental error is taken to be 10–15%. The only exception is low-density polyethylene (LDPE), which fits the model even though it is rubbery at room temperature. Ward and co-workers have previously suggested[44,45] that the model may fail if there is significant change in morphology during the orientation process, as in the case of PP. However, our ultrasonic result on PP mentioned above shows that the model may still be applicable when there are morphological changes. In summary, it seems that the general rule based on the relaxation behaviour of the amorphous

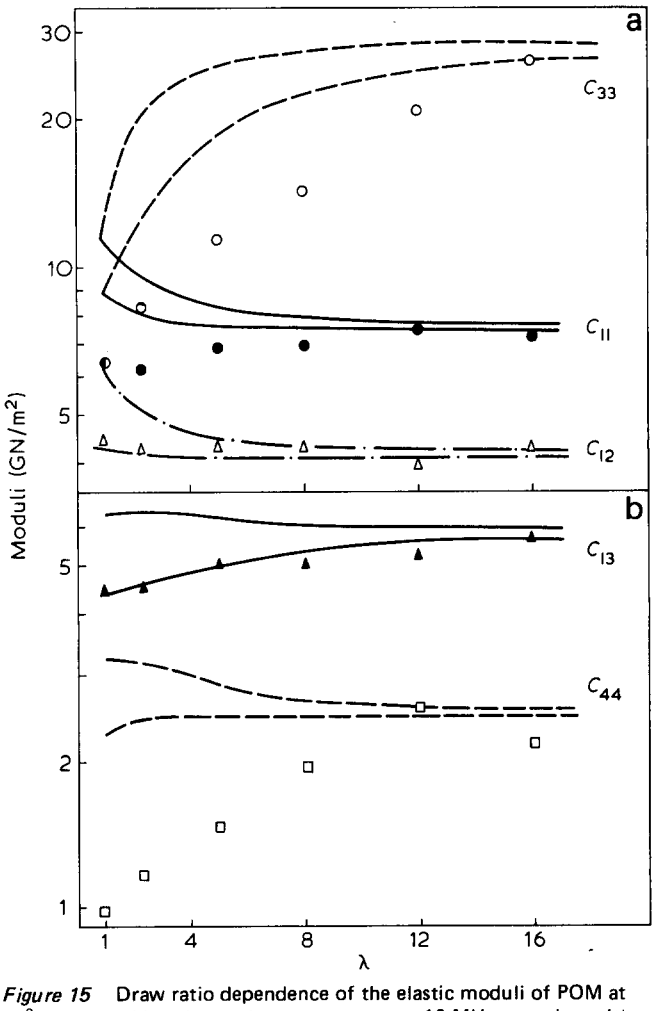

Figure 15 Draw ratio dependence of the elastic moduli of POM at 60°C obtained by ultrasonic measurement at 10 MHz, together with Voigt and Reuss bounds calculated from the aggregate model. Legends are as for *Figure 14*

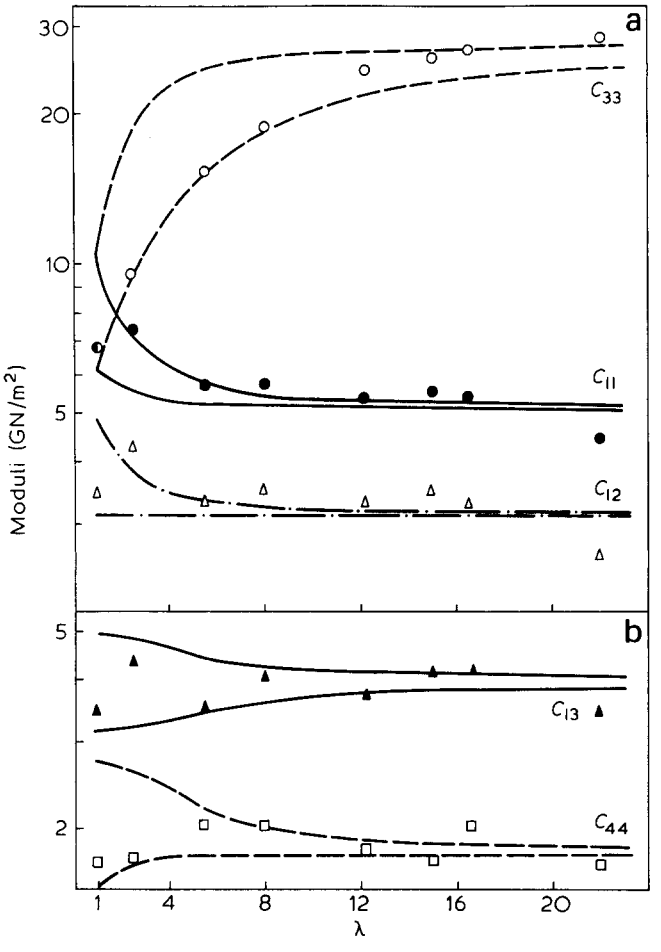

Figure 16 Draw ratio dependence of the elastic moduli of PP at 0°C obtained by ultrasonic measurement at 10 MHz, together with Voigt and Reuss bounds calculated from the aggregate model. Legends are as for *Figure 14*

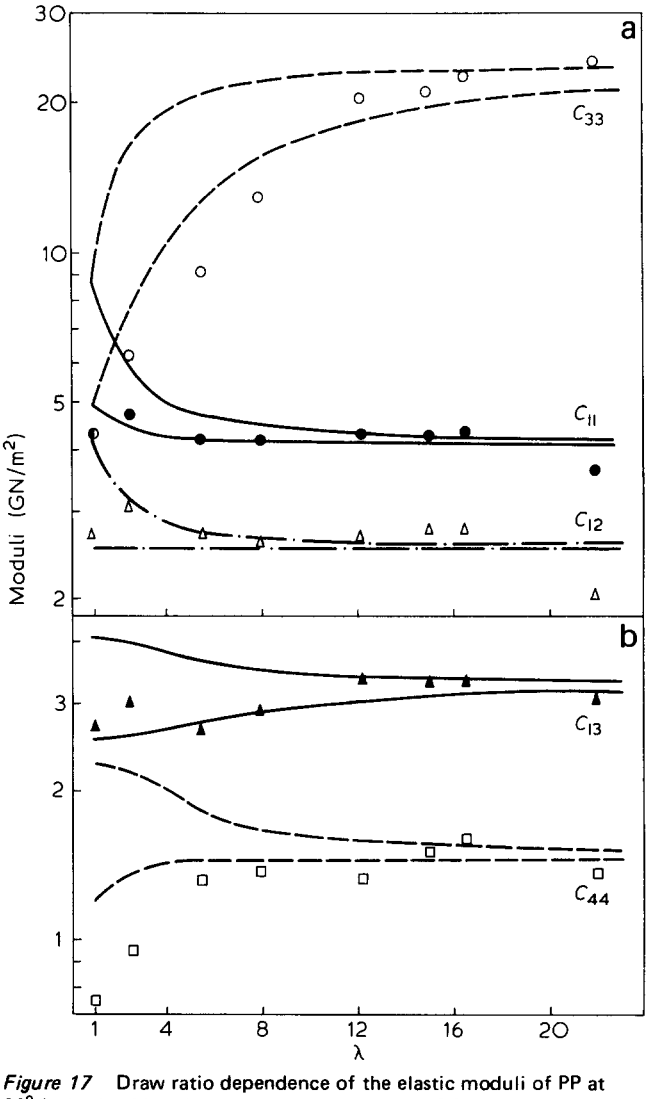

Figure 17 Draw ratio dependence of the elastic moduli of PP at 60°C obtained by ultrasonic measurement at 10 MHz, together with Voigt and Reuss bounds calculated from the aggregate model. Legends are as for *Figure 14*

phase should be sufficient to cover (or is at least consistent with) all available data, with the noted exception of LDPE. One may also mention that the moduli of a number of amorphous[44] or slightly crystalline[21] polymers are known to be consistent with the aggregate model, as one would expect of one-phase materials.

CONCLUSIONS

Our studies show that the process of orientation produces two major changes in semicrystalline polymers.

(a) the preferential alignment of molecular chain axes along the draw-axis, which is mainly responsible for the marked increase in the modulus C_{33} and a slight decrease in C_{11};

(b) a general decrease in molecular mobility, such that the relaxation peaks associated with the amorphous region decrease in height and shift upwards in temperature, and the drop of moduli at the corresponding relaxations becomes smaller. Consequently both the tensile and the shear moduli show a much stronger λ-dependence at high temperature.

The low-frequency and ultrasonic data show reasonably good agreement when compared with each other by use of the time–temperature equivalence rule. This provides firm evidence that the rule is generally applicable to oriented polymers over fairly wide ranges of frequency. It is also satisfactory that the drawn semi-

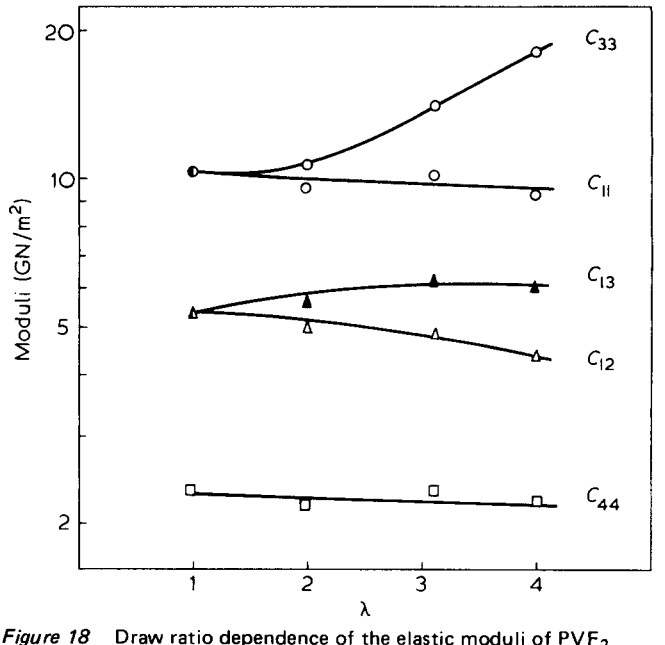

Figure 18 Draw ratio dependence of the elastic moduli of PVF_2 at 0°C obtained by ultrasonic measurement at 10 MHz. Solid lines are smooth curves drawn through the experimental points

crystalline polymer follows the predictions of a one-phase model (the aggregate model) at temperatures below the glass-transition, when there is relatively little difference in stiffness between its amorphous and crystalline phases, but not at higher temperature when the amorphous phase becomes rubbery. This agrees with previous work on both semicrystalline and amorphous polymers. However, the analysis remains qualitative in character, and considerable progress in our understanding of the structure of oriented polymers, and in the development of a theoreti-

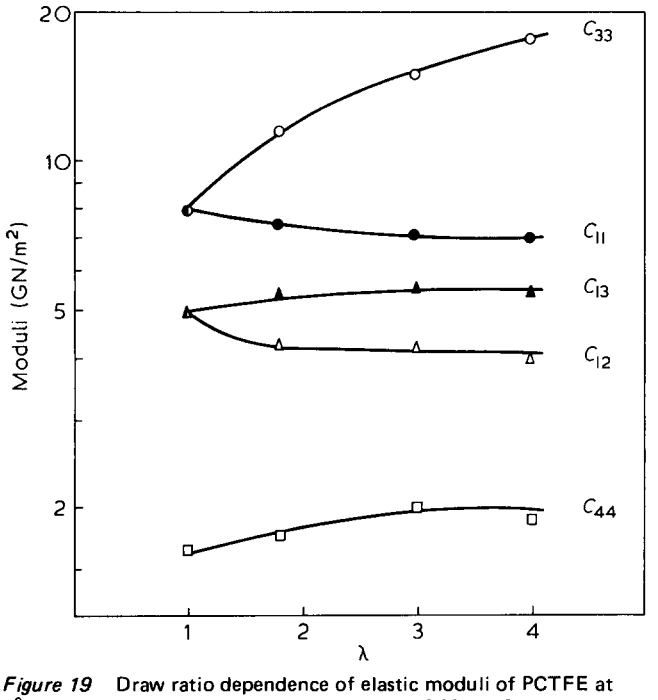

Figure 19 Draw ratio dependence of elastic moduli of PCTFE at 0°C obtained by ultrasonic measurement at 10 MHz. Solid lines are smooth curves drawn through the experimental points

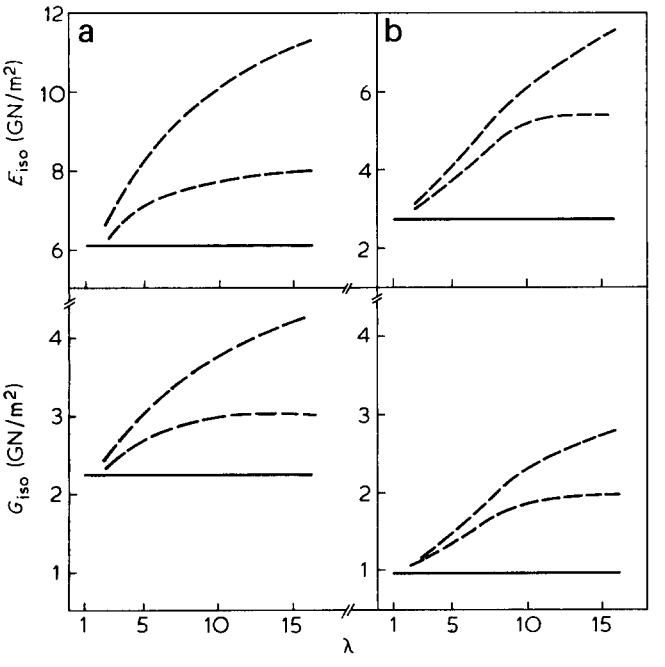

Figure 20 The Young's (E_{iso}) and shear (G_{iso}) modulus of the isotropic sample (shown as ——) of POM at (a) 0°C and (b) 60°C. Isotropic bounds for these moduli calculated according to the aggregate model from the moduli of each oriented sample of POM are shown as — — — —

Table 1 The Young's moduli E_0, E_{90} and shear moduli $G(=C_{44})$ of POM and PP at 0 and 60°C, and of PVF_2 and PCTFE at 0°C, as determined by ultrasonic measurements

POM 0°C	λ = 1	2.3	5	8	12	16
E_0	6.1	8.7	14.7	20.4	27.5	33.0
E_{90}	6.1	5.3	6.0	6.0	6.5	6.7
G	2.25	2.82	3.6	4.0	3.2	3.1
POM 60°C	**λ = 1**	**2.3**	**5**	**8**	**12**	**16**
E_0	2.73	4.1	6.5	10.4	15.4	20.6
E_{90}	2.73	2.85	3.6	4.0	4.57	4.4
G	0.97	1.2	1.5	1.96	2.55	2.1

PP 0°C	λ = 1	2.5	5.5	8	12.2	15	16.5	22
E_0	4.5	6.4	12.4	15.6	21.0	22.3	22.8	24
E_{90}	4.5	4.4	3.7	3.5	3.4	3.3	3.3	2.9
G	1.68	1.72	2.03	2.02	1.81	1.72	2.04	1.70
PP 60°C	**λ = 1**	**2.5**	**5.5**	**8**	**12.2**	**15**	**16.5**	**22**
E_0	2.09	3.23	7.1	10.3	15.2	17.9	17.7	21.1
E_{90}	2.09	2.65	2.50	2.54	2.57	2.50	2.65	2.39
G	0.75	0.95	1.31	1.37	1.44	1.50	1.60	1.36

PVF_2 0°C	λ = 1	2	3	4
E_0	6.4	6.4	9.6	12.9
E_{90}	6.4	6.1	6.5	6.3
G	2.36	2.18	2.36	2.24
PCTFE 0°C	**λ = 1**	**1.8**	**3**	**4**
E_0	3.9	6.2	9.9	13.0
E_{90}	3.9	4.2	4.4	4.6
G	1.65	1.75	2.03	1.88

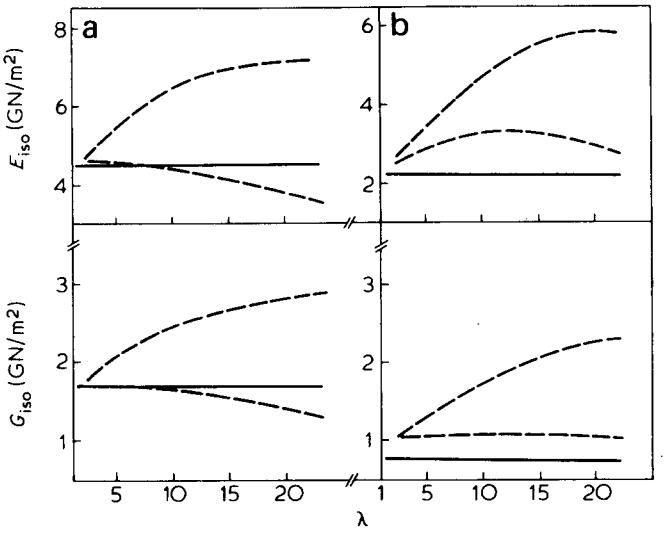

Figure 21 The Young's (E_{iso}) and shear (G_{iso}) modulus of the isotropic sample (shown as ——) of PP at (a) 0°C and (b) 60°C. Isotropic bounds for these moduli calculated according to the aggregate model from the moduli of each oriented sample of PP are shown as — — — —

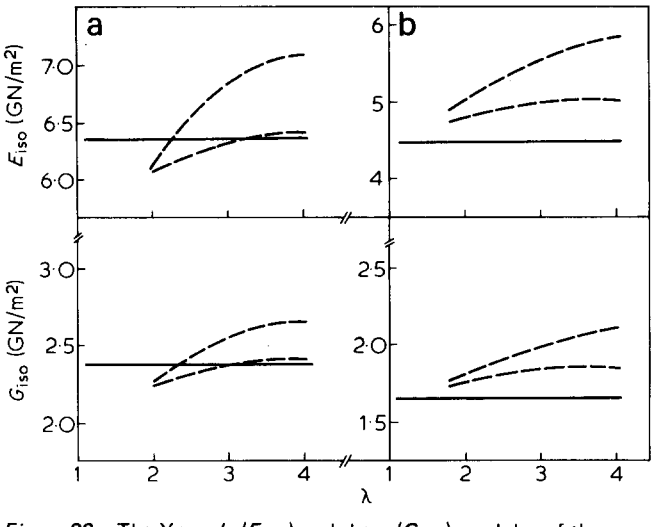

Figure 22 The Young's (E_{iso}) and shear (G_{iso}) modulus of the isotropic sample (shown as ——) of (a) PVF_2 at 0°C and (b) PCTFE at 0°C. Isotropic bounds for these moduli calculated according to the aggregate model from the moduli of each oriented sample of the respective polymers are shown as — — — —

cal framework for its description would be required before a detailed calculation of the effects mentioned can be made.

ACKNOWLEDGEMENT

We are grateful to Hoechst Co., 3M Co. and DuPont Co. for supplying the samples of polypropylene, polychlorotrifluoroethylene and polyoxymethylene, respectively.

REFERENCES

1 For a review of the work before 1974 see Hadley, D. W., pp. 290, 'Structure and Properties of Oriented Polymers', (Ed. I. M. Ward) Applied Science Publishers Ltd, London, 1975
2 Williams, T. *J. Mater. Sci.* 1973, **8**, 59
3 Gibson, A. G., Ward, I. M., Cole, B. N. and Parsons, B. *J. Mater. Sci.* 1974, **9**, 1193
4 Capaccio, G. and Ward, I. M. *Polymer* 1974, **15**, 233
5 Cansfield, D. L. M., Capaccio, G. and Ward, I. M. *Polym. Eng. Sci.* 1976, **16**, 721
6 Clark, E. S. and Scott, L. S. *Polym. Eng. Sci.* 1974, **14**, 682
7 Taylor, W. N. and Clark, E. S. *Polym. Preprints* 1977, **18**, 332
8 Weeks, N. E. and Porter, R. S. *J. Polym. Sci. Phys. Edn.* 1974, **12**, 635
9 Capiati, N. J. and Porter, R. S. *J. Polym. Sci., Phys. Edn.* 1975, **13**, 1177
10 Mead, W. T., Desper, C. R. and Porter, R. S. *J. Poly. Sci., Phys. Edn.* 1979, **17**, 859
11 Mead, W. T., Zachariades, A. E., Shimada, T. and Porter, R. S. *Macromolecules* 1979, **12**, 473
12 Brew, B. and Ward, I. M. *Polymer* 1978, **19**, 1338
13 Coates, P. D. and Ward, I. M. *J. Polym. Sci., Phys. Edn.* 1978, **16**, 2031
14 Brew, B., Clements, J., Davies, G. R., Jakeways, R. and Ward, I. M. *J. Polym. Sci., Phys. Edn.* 1979, **17**, 351
15 Capaccio, G. and Ward, I. M. *PRI Proc. Int. Conference on Deformation, Yield and Fracture of Polymers*, Cambridge, March 1976
16 Smith, J. B., Davies, G. R., Capaccio, G. and Ward, I. M. *J. Polym. Sci., Phys. Edn.* 1975, **13**, 2331
17 Gibson, A. G., Davies, G. R. and Ward, I. M. *Polymer* 1978, **19**, 683
18 Chan, O. K., Chen, F. C., Choy, C. L. and Ward, I. M. *J. Phys. D: Appl. Phys.* 1978, **11**, 617
19 Datta, P. K. and Pethrick, R. A. *Polymer* 1978, **19**, 145
20 Rider, J. G. and Watkinson, K. M. *Polymer* 1978, **19**, 645
21 Rawson, F. F. and Rider, J. G. *J. Phys. D: Appl. Phys.* 1974, **7**, 41
22 Markham, M. F. *Composites* 1970, **1**, 145
23 Dean, G. D. and Turner, P. *Composites* 1973, **4**, 174
24 Hammer, C. F., Koch, T. A. and Whitney, J. F. *J. Appl. Polym. Sci.* 1959, **1**, 169
25 Lee, W. A. and Rutherford, R. A. 'Polymer Handbook', (Eds J. Brandrup and E. H. Immergut) Interscience, New York, 1975
26 Hoffman, J. D. and Weeks, J. C. *J. Res. Nat. Bur. Stand. USA* 1958, **60**, 465
27 Nakagawa, K. and Ishida, *J. Polym. Sci.* (*A*-2) 1973, **11**, 2153
28 Arridge, R. G. C., Barham, P. J., Farrell, C. and Keller, A. *J. Mater. Sci.* 1976, **11**, 788
29 Gray, R. W. and McCrum, N. G. *J. Polym. Sci.* (*A*-2) 1969, **7**, 1329
30 McCrum, N. G., Read, B. E. and Williams, G. 'Annelastic and Dielectric Effects in Polymeric Solids' John Wiley & Sons, London, 1967
31 Musgrave, M. J. P. *Rep. Prog. Phys.* 1959, **22**, 77
32 Boyer, R. F. *J. Poly. Sci.: Symposium* 1975, **50**, 189
33 Lando, J. B. and Doll, W. W. *J. Macromol. Sci.* 1968, **B2(2)**, 205
34 Kwan, S. F., Chen, F. C. and Choy, C. L. *Polymer* 1975, **16**, 481
35 Eby, R. K. *J. Chem. Phys.* 1962, **37**, 2785
36 Kono, R. *J. Phys. Soc. Japan* 1961, **16**, 1580
37 Stein, R. S. and Wilks, G. L. 'Structure and Properties of Oriented Polymers' (Ed. I. M. Ward) Applied Science Publishers Ltd, London, 1975, p 57
38 Peterlin, A. *Kolloid Z.* 1969, **233**, 857
39 Peterlin, A. *J. Mater. Sci.* 1971, **6**, 490
40 Takayanagi, M., Imada, K. and Kajiyama, *J. Polym. Sci.* (*C*) 1966, **15**, 263
41 Gibson, A. G., Greig, D., Sahota, M., Ward, I. M. and Choy, C. L. *J. Polym. Sci. (Polym. Lett. Edn)* 1977, **15**, 183
42 Ward, I. M. *Proc. Phys. Soc.* 1962, **80**, 1176
43 Ward, I. M. 'Mechanical Properties of Solid Polymers' John Wiley, London, 1971
44 Hadley, D. W. and Ward, I. M., pp. 264, 'Structure and Properties of Oriented Polymers', (Ed. I. M. Ward) Applied Science Publishers Ltd, London, 1975
45 Hadley, D. W., Pinnock, P. R. and Ward, I. M. *J. Mater. Sci.* 1969, **4**, 152

APPENDIX

For the least-squares fit of equation (3) to N experimental points $(x_i,y_i)(i=1,2,\ldots,N)$ one applies the usual criterion that

$$S=\sum_{i=1}^{N}(y_i^2+a_1x_iy_i+a_2y_i^2+a_3y_i+a_4) \qquad \text{(A1)}$$

should be minimized with respect to the choice of a_n, leading to the condition

$$\frac{\partial S}{\partial a_n}=0 \quad (n=1,2,3) \tag{A2}$$

$a_4(=a_1a_3-a_2)$ is a dependent function of the other three variables a_i and cannot be independently varied, which makes the solution of (A2) considerably more complicated than usual. After simplification (A2) results in the following quintic equation for a_3:

$$p^2(f_4a_3+f_5)+pq(2f_3a_3+f_2)+q^2(f_7a_3+f_8)=0 \tag{A3}$$

where

$$p=-(f_3a_3^2+f_2a_3+f_6) \tag{A4}$$

$$q=f_4a_3^2+2f_5a_3+f_1$$

The coefficients f_n $(n=1,\ldots,8)$ are:

$$f_1=ru_{31}{}^2+v_{22}$$

$$f_2=ru_{21}u_{31}+u_1u_4+2v_{12}$$

$$f_3=ru_{30}u_{21}+v_{11}$$

$$f_4=ru_{30}{}^2+v_{20}$$

$$f_5=ru_{30}u_{31}+v_{21}$$

$$f_6=ru_{31}u_{22}+v_{13}$$

$$f_7=ru_{21}{}^2+v_{02}$$

$$f_8=ru_{21}u_{22}+v_{03} \tag{A5}$$

where

$$v_{mn}=\sum_{i=1}^{N}x_i^my_i^n$$

$$u_{mn}=r^2(v_{mn}-v_{m-1\ n})$$

$$r=1/(2v_{30}-v_{20}-v_{40}) \tag{A6}$$

(A3) can be solved numerically for a_3, from which p, q, a_1 and a_2 can be obtained:

$$a_1=p/q \tag{A7}$$

$$a_2=r^2(u_{30}a_1a_3+u_{31}a_1+u_{21}a_3+u_{22}) \tag{A8}$$

It should be mentioned that the above solution for a_n $(n=1,2,3)$ is not always unique even within the physically reasonable ranges of the elastic moduli, because equation (A2) only defines a local stationary point for S. When one actually finds two local minima it is necessary to compare the values of S at these two points to find the absolute minimum in order to obtain the best fit to data.